Phys Chem Minerals (2006)
DOI 10.1007/s00269-005-0052-z

ORIGINAL PAPER

Innokenty Kantor · Leonid Dubrovinsky
Catherine McCammon · Anastasia Kantor
Sakura Pascarelli · Giuliana Aquilanti
Wilson Crichton · Maurizio Mattesini
Rajeev Ahuja · Jailton Almeida · Vadim Urusov

Pressure-induced phase transition in $Mg_{0.8}Fe_{0.2}O$ ferropericlase

Received: 8 August 2005 / Accepted: 1 November 2006

Abstract Combined X-ray powder diffraction, Mössbauer, and XANES spectroscopy in situ experiments revealed the transformation of cubic $(Mg_{0.8}Fe_{0.2})O$ ferropericlase to a rhombohedrally distorted phase at 35(1) GPa and room temperature. The Mössbauer spectroscopy results show that the rhombohedral distortion does not involve magnetic ordering. Combined with data from the literature, our results imply that the cubic to rhombodedral transition occurs in (Mg,Fe)O under conditions of non-hydrostatic stress over a wide range of composition ($0.2 \leq x_{Fe} \leq 1$).

Keywords Diamond anvil cell · Ferropericlase · High pressure

Introduction

Transition metal monoxides (MnO, FeO, CoO, and NiO) are of great interest for solid-state physics and technology due to their magnetic, electronic, and structural properties. Phase transitions from cubic to distorted structures with lower symmetries are known to occur in all of these oxides (Rooksby 1948; Willis and Rooksby 1953; Saito et al. 1966; Morosin 1970). At ambient pressure, structural transition temperatures appear to coincide with Néel temperatures. It was suggested (Smart and Greenwald 1951) that these crystallographic deformations are a consequence of the exchange interactions which result from antiferromagnetic ordering. Also, ab initio calculations of FeO and MnO show that a magnetically ordered state stabilizes trigonal structures relative to cubic structures at zero temperature and atmospheric pressure (Fang et al. 1999; Gramsch et al. 2003). At elevated pressures, MnO, FeO, and CoO also undergo the same type of rhombohedral distortion: MnO at ca. 35 GPa (Yoo et al. 2005), FeO at ca. 16 GPa (Shu et al. 1998a) and CoO at ca. 43 GPa (Guo et al. 2002). The rhombohedral distortion of FeO is thought to be a second-order transition with negligible volume change at the transition, where the space group of the trigonal phase is a subgroup of the high-symmetry cubic phase (Shu et al. 1998a); however it could also be a weak first-order transition. High-pressure Mössbauer spectroscopic studies of FeO at widely spaced pressure intervals showed the Néel transition to occur in a similar pressure range (Nasu 1994), and suggested that these structural transitions resulted from an increase of the Néel temperature with pressure. However a recent high-pressure Mössbauer and ultrasonic elasticity study of FeO revealed a magnetic transition in FeO at about 5 GPa, which differs significantly from the structural transition pressure (Kantor et al. 2004a, b). One approach to elucidate the relation between the magnetic and structural transitions is to eliminate magnetic interactions by diluting FeO in a non-magnetic isostructural compound (e.g., MgO and the mineral periclase). MgO is extremely stable in the rock-salt structure and is not observed to undergo any structural transitions up to at least 227 GPa at ambient temperature (Duffy et al. 1995). The rhombohedral distortion in $(Mg_xFe_{1-x})O$ solid solution (the mineral ferropericlase when $x > 0.5$ and magnesiowüstite when $x \leq 0.5$) was

I. Kantor (✉) · L. Dubrovinsky · C. McCammon · A. Kantor
Bayerisches Geoinstitut, Universität Bayreuth,
95440 Bayreuth, Germany
E-mail: Innokenty.Kantor@Uni-Bayreuth.DE
Tel.: +49-921-553735
Fax: +49-921-553769

S. Pascarelli · G. Aquilanti · W. Crichton
European Synchrotron Radiation Facility,
6 Rue J. Horowitz, BP 220, 38043 Grenoble Cedex 9, France

M. Mattesini · R. Ahuja · J. Almeida
Condensed Matter Theory Group, Uppsala University,
256, 751 05 Uppsala, Sweden

M. Mattesini
Departamento de Física de la Materia Condensada,
Universidad Autónoma de Madrid, 28049 Madrid, Spain

V. Urusov
Department of Crystallography, Moscow State University,
GSP-2, Lenin Hills, 119992 Moscow, Russia

observed over a relatively wide composition range (Kantor et al. 2005; Kondo et al. 2002; Mao et al. 2002; Shu et al. 1998b). Some controversy exists regarding the minimum iron content that allows lattice distortion in ferropericlase: it was recently reported (Lin et al. 2003) that no phase transition occurs in $(Mg_{0.39}Fe_{0.61})O$ up to 102 GPa.

$(Mg_xFe_{1-x})O$ ferropericlase with $x \approx 0.8$ is believed to be the second most abundant phase in the Earth's lower mantle after $(Mg,Fe)SiO_3$ perovskite, and therefore its properties and stability field are important for geophysical and geochemical models of the Earth's deep interior (Badro et al. 2003; Dubrovinsky et al. 2000b; Lin et al. 2003; Wentzkovitch et al. 2004). We performed an in situ investigation of the behavior of $(Mg_{0.8}Fe_{0.2})O$ at elevated pressure in diamond anvil cells (DACs) using Mössbauer spectroscopy (MS) as a direct method to probe magnetic properties of the material at high pressures, X-ray Fe K_α-edge absorption spectroscopy (XANES) as a method to probe the local environment of iron atoms, and X-ray powder diffraction (XRD) to provide information about long-range order and symmetry of the material.

Methodology

Experiment

Two samples, FP-1 and FP-2, with nominal composition $Mg_{0.8}Fe_{0.2}O$ were used in the experiments as starting material, and are the same as used in previous experiments (McCammon et al. 1998). The two samples have the same nominal composition, and differ only in ferric iron content. The first sample was synthesized by mixing stoichiometric amounts of MgO and Fe_2O_3 (50% enriched with ^{57}Fe), heating overnight at 1,200°C in reducing conditions ($\log fO_2 = -17.4$) using a CO/CO_2 gas-flow furnace and quenching into water. This low ferric iron sample ($Fe^{3+}/\sum Fe = 0.043$) is hereafter referred to as FP-1. A high ferric iron sample (FP-2) was synthesized by re-equilibrating part of sample FP-1 at higher oxygen fugacity ($\log fO_2 = -8.9$) and 1,200°C, and quenching into water ($Fe^{3+}/\sum Fe = 0.074$). Lattice constants are $a = 4.2389(5)$ and $4.2348(5)$ Å for samples FP-1 and FP-2, respectively. After the experiments, the chemical composition of the quenched samples was checked by scanning electron microscopy and X-ray microprobe: no changes in chemical composition were detected, and no evidence for chemical inhomogeneity on the length scale of the measurements (ca. 1 μm) was observed.

High-pressure measurements were performed in a three-pin (MS) or four-pin (X-ray absorption and X-ray diffraction) modified Merrill–Basset design DAC (Dubrovinskaia and Dubrovinsky 2003), mounted with gem-quality diamonds with 250-μm culets. A rhenium gasket with initial thickness of 260 μm was preindented to about 20–40 μm, and a 125-μm-diameter hole was drilled in the gasket and filled with sample powder. Several small ruby chips were also loaded in the sample chamber for pressure measurements and estimations of pressure gradients (Mao et al. 1986). No pressure-transmitting medium was used. To relieve stresses at high pressure, samples were scanned for about 30 s at several stages during the experiment using an infrared laser at low power at temperatures below 1,000 K. Thermal radiation from the sample was detected by an infrared-sensitive camera, confirming that the sample in the DAC was indeed heated. Laser heating was performed at several pressures: 25, 36, 49, and 55 GPa.

^{57}Fe Mössbauer spectra (MS) of samples FP-1 and FP-2 were recorded at room temperature in transmission mode on a constant acceleration Mössbauer spectrometer using a high specific activity ^{57}Co point source in a Rh-matrix. The beam diameter (> 500 μm) was larger than the sample diameter, so absorption was measured from the entire sample volume. The velocity scale was calibrated relative to a 25-μm α-Fe foil. Collection time for each spectrum varied from 12 to 24 h. Pressure was measured before and after each run and then averaged. The typical pressure drift during Mössbauer measurements was less than or about 1 GPa.

The XAS measurements were carried out on the dispersive XAS beamline ID24 at the ESRF. The gap of the undulator was optimized to have the maximum of the first harmonic in the energy range 7,000–7,500 eV. The optics comprised a pair of curved SiC mirrors in a Kirkpatrick Baez geometry at a grazing incidence angle of 3 mrad, followed by a Si(111) polychromator crystal in the Bragg geometry and an additional vertically focusing Si mirror at a grazing incidence of 3.5 mrad (Pascarelli et al. 2004). The size of the beam on the sample was approximately 10×10 μm^2 full width at half maximum (FWHM). Spectra were recorded using a CCD-based position sensitive detector in the energy range 7,070–7,330 eV. Pixel-energy calibration was obtained by measuring spectra on a reference Fe foil sample.

Angle-dispersive X-ray diffraction measurements (XRD) were made at beamline ID30 at the European Synchrotron Radiation Facility (ESRF). The MAR 345 image-plate system at 450 mm distance from the sample was used as a detector. The size of the beam on the sample was approximately 10×9 μm^2 FWHM. All samples measured with XAS were also studied at the same pressures by XRD.

Calculations

Theoretical calculations of the X-ray absorption spectra were based on an ab initio self-consistent real space multiple scattering method (Ankudinov et al. 1998, 2002; Rehr and Albers 2000; Zabinsky et al. 1995) for a cluster of atoms centered on the absorbing ion. The electric-dipole approximation was employed, meaning that only the transitions between the atomic core wave

functions with orbital angular momentum l to the l+1 components of the normalized continuum wave functions were considered. The Hedin–Lundqvist (Hedin and Lindqvist 1971) self-energy model was used for the exchange correlation potential. The computed XANES spectra were consistent with the final-state rule (von Barth and Grossman 1982), where a core hole is present in the charge density. Absorption Fe K-edge spectra were calculated for the MgO rock-salt structure where 20% of the Mg atoms were randomly substituted by the Fe ions. All the multi-scattering calculations were conducted on a spherical atomic cluster of radius of 10 Å.

In a solid solution, atoms are normally shifted from their regular positions due to the non-homogeneous environment. We calculated relaxed atomic coordinates in the $(Mg_{0.8}Fe_{0.2})O$ solid solution using a simple pair potentials method incorporating the GULP (Gale 1997) code. A 4×4×4 *fcc* supercell containing 512 ions with randomly distributed Mg and Fe in the cation sublattice was used for relaxation calculations and the resulting equilibrium atomic coordinates were transferred into the cluster for further ab initio XANES spectra calculations. Parameters of the Buckingham interatomic pair potentials for Fe–O and O–O interactions were taken from Minervini and Grimes (Minervini and Grimes 1999); and parameters of Mg–O short-range potential were fitted to reproduce the experimental structure and elasticity of MgO (Zha et al. 2000), resulting in $A_{Mg-O} = 805.54$ eV and $\rho_{Mg-O} = 0.3246$ Å. The presence of ferric iron in the ferropericlase structure, as well as charge-compensating vacancies, was ignored in these calculations.

Results

Mössbauer spectroscopy

The MS of samples FP-1 and FP-2 were collected at pressures up to 56 GPa. The spectra are consistent with single-phase (Mg,Fe)O, and no evidence for chemical inhomogeneity (e.g., FeO-rich regions) was found. A typical Mössbauer spectrum of sample FP-1 at 47 GPa is shown in Fig. 1 (inset). We deconvoluted the MS according to the model, incorporating two Lorentzian quadrupole doublets, one for Fe^{2+} and one for Fe^{3+} sites (Dobson et al. 1998), where the amount of Fe^{2+} and Fe^{3+} was determined based on the absorption area of the relevant doublet. Within the pressure range from 3 to 56 GPa, the proportion of Fe^{3+} in each sample remains essentially constant: the $Fe^{3+}/\sum Fe$ ratio fluctuates around 4.7% for sample FP-1 and 7.7% for sample FP-2 within the estimated error of 0.4%. We did not observe any significant difference in the high-pressure behavior between the FP-1 and FP-2 samples within the uncertainty of the measurements. The isomer shift of the main doublet depends linearly on pressure with a slope of about −0.003 mm/s per GPa within the studied pressure range. We observed a strong non-monotonous pressure dependence of the quadrupole splitting: it increases up to pressures of about 36–37 GPa and decreases at higher pressures (Fig. 1). No difference between compression and decompression paths was observed, and the quadrupole splitting changes described above were completely reversible. Quadrupole splitting is a sensitive indicator of the distortion of the local iron environment. For example, in $FeSiO_3$ clinoferrosilite the distortion of the $M2(Fe^{2+})$ octahedron is coupled to a rapid decrease of quadrupole splitting (McCammon and Tennant 1996). We infer that the changes in quadrupole splitting of samples FP1 and FP2 are also due to changes in the distortion of the local Fe^{2+} environment. No evidence of magnetic ordering or line broadening in MS were observed up to the highest pressure reached in this study (56 GPa). As was shown for FeO (Kantor et al. 2004b), even when magnetic ordering is incomplete and the Mössbauer spectrum does not show a resolved six-line structure, magnetic ordering can be easily detected by significant broadening of absorption lines: neither effect was observed in the high-pressure MS of the ferropericlase samples.

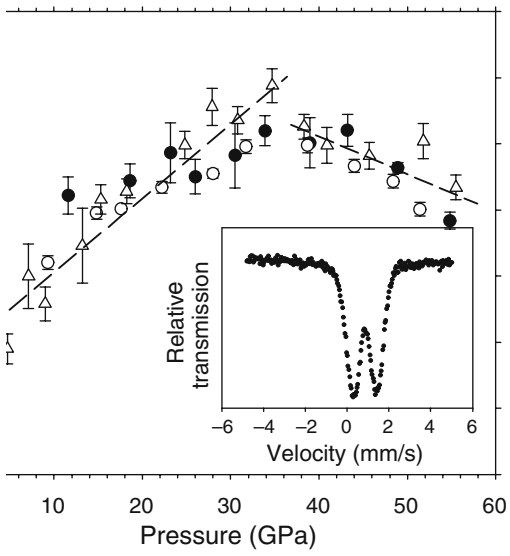

Fig. 1 Quadrupole splitting of the dominant doublet derived from room temperature Mössbauer spectra (MS) as a function of pressure. *Solid circles*, compression path of sample FP-1; *open circles*, decompression path of sample FP-1; *triangles*, compression path of sample FP-2. *Dashed lines* are guides for the eye. *Inset*: MS of sample FP-1 at 47(1) GPa. The velocity scale is relative to α-Fe

X-ray absorption spectroscopy

X-ray absorption spectra were collected from 0 to 59 GPa at room temperature in the DAC. Selected spectra at different pressures are shown in Fig. 2. In general, Fe K-edge XANES spectra of ferropericlase are similar to Co and Ni K-edge XANES spectra of (Co,Mg)O and (Ni,Mg)O solid solutions (Kuzmin et al. 1997). Upon compression, the peaks in the XANES

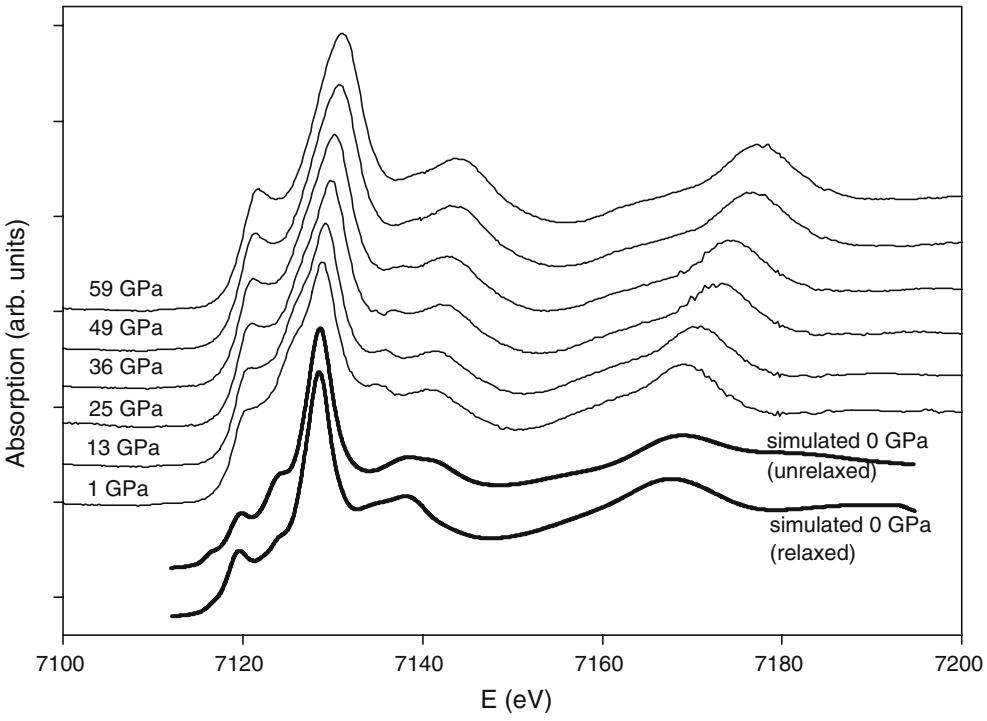

Fig. 2 Experimental XANES spectra of sample FP-1 at various pressures (six upper curves) and simulated XANES spectra at zero pressure with relaxed and unrelaxed atomic coordinates (two lower curves—see the text for details). Spectra are shifted vertically for clarity

spectra of sample FP-1 shift to higher energies, mainly due to increasing electron density at the Fe nucleus (no XANES or XRD spectra were collected for sample FP-2 due to time constraints and the observed lack of significant influence of Fe^{3+} concentration on the transition seen in Mössbauer data). Changes in the spectra as a function of pressure can be highlighted using $\delta\mu/\delta E$ derivatives (Fig. 3), and show that, in particular, the intensity minimum at ~7,127 eV disappears near 36 GPa. One of the most important characteristics of

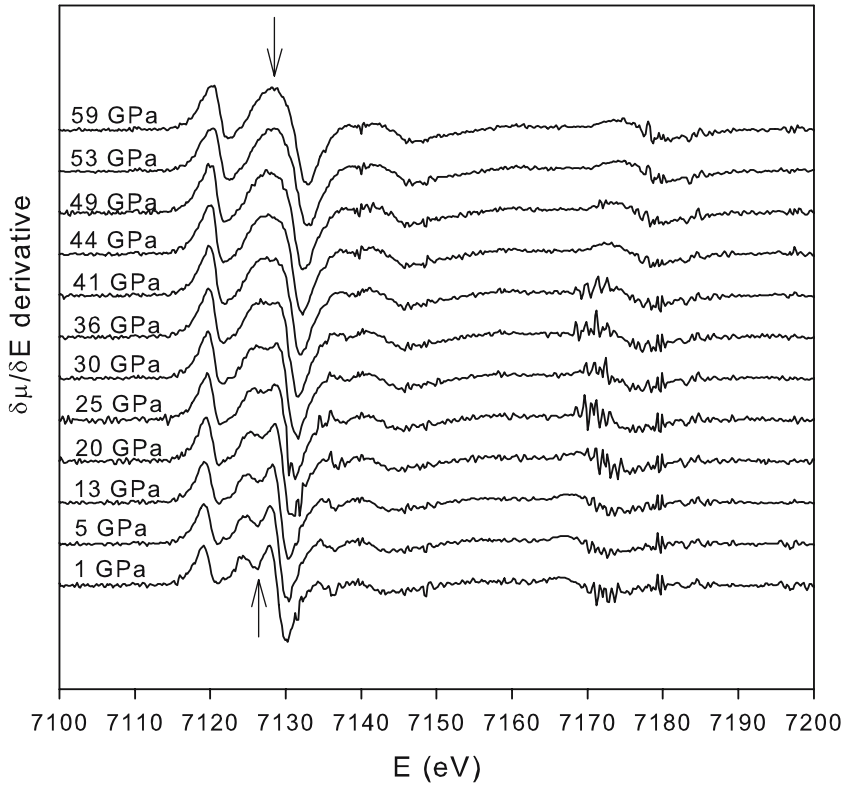

Fig. 3 $\delta\mu/\delta E$ derivatives of experimental XANES spectra from sample FP-1. *Arrows* indicate the region in which changes are observed at about 36 GPa

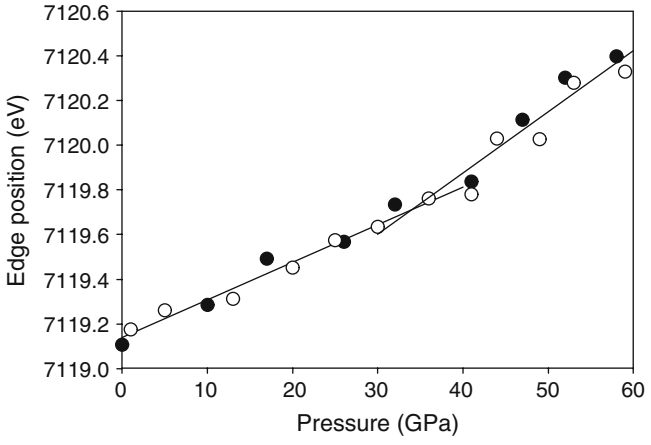

Fig. 4 X-ray Fe K_α-edge position derived from experimental XANES spectra of sample FP-1 as a function of pressure. *Solid and open symbols* represent compression and decompression paths, respectively. *Lines* are least-square linear fits to the high- and low-pressure data with intersection at 34 GPa

XANES spectra is the position of the absorption edge (usually defined as a maximum of the first derivative), which is sensitive to the valence state and chemical bonding of the absorbing atom (Srivastava and Nigam 1973; Lytle et al. 1988). The absorption-edge position of ferropericlase increases with increasing pressure, but not monotonously (Fig. 4). If all data that are clearly below ($P < 30$ GPa) and above ($P > 40$ GPa) the transition are fitted separately to linear models, the lines intersect at 34 GPa. We observed that all changes to the spectra were completely reversible and showed no pressure hysteresis, and the XANES spectrum of the recovered sample was identical to that of the starting material.

We performed ab initio calculations of the XANES spectra in order to compare them with those from the experiments. Due to the difficulty of ab initio calculations to account for the strong electron correlations in these types of oxides, we do not expect the calculated positions of all spectral features to be correctly determined, but it is instructive to investigate if at least the topological features can be reproduced. The first calculation was made assuming that all ions are located in the regular positions of the cubic lattice. With this assumption, the "unrelaxed" Fe K-edge absorption spectrum is in generally good qualitative agreement with the experimental data, where the most significant qualitative deviation is a small feature at about 7,135 eV that is absent in the calculated spectrum (Fig. 2). In order to improve our calculations, we modeled a more physically realistic case when atoms are shifted from their regular positions. We calculated relaxed coordinates of atoms using simple pair atomic potentials, and then used these relaxed coordinates for ab initio calculations of the XANES spectrum. Although the average shift of atoms from their regular positions was small (about 0.03 Å), the qualitative agreement of the calculated XANES spectrum with the experimental spectra is improved (Fig. 2, 5). Kizler (1992) described a mathematical procedure to treat XANES spectra to make features of the spectra more pronounced, i.e., taking a difference between the initial curve and a 5-eV running average (Fig. 5). As seen from Fig. 5, the relaxed spectrum is in better agreement with the experimental spectra, and the feature at ~7,135 eV appears as indicated by the arrow.

X-ray diffraction

The X-ray diffraction data of sample FP-1 can be fit perfectly to a cubic rock-salt structure up to 35 GPa. At pressures higher than 36 GPa, some of the diffraction

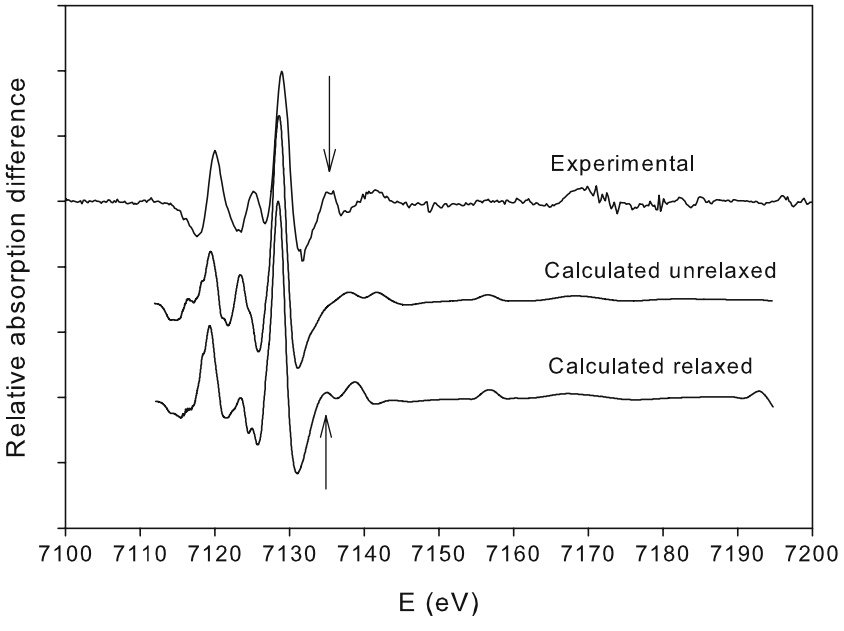

Fig. 5 Difference between XANES spectra and 5-eV running averages (see the text) for experimental and calculated spectra at zero pressure. The *arrows* indicate the feature at ~7,135 eV discussed in the text

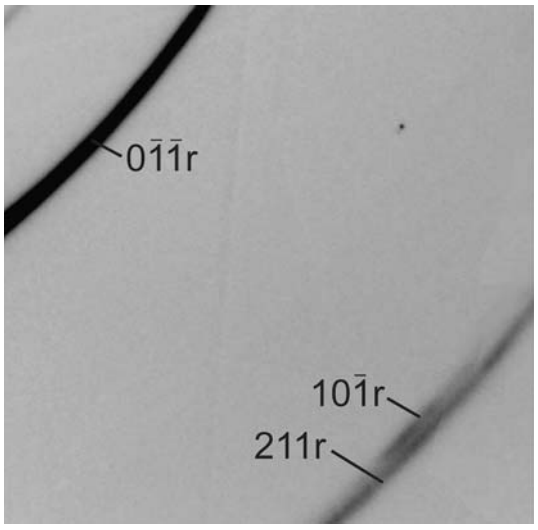

Fig. 6 Part of MAR345 diffraction image of sample FP-1 at 44(1) GPa. Reflection indices are for a rhombohedral lattice ($a=b=c$, $\alpha=\beta=\gamma\neq 60°$)

peaks rapidly start to become broadened. The transition from a cubic to a rhombohedral structure should result in the splitting of 111_c, 220_c, and 311_c cubic reflections, while the most intense 200_c cubic reflection remains unsplit (Mao et al. 2002; Shu et al. 1998a) (hereafter we use the subscripts "c" and "r" to denote the cubic and rhombohedral cells, respectively). From the X-ray diffraction images, we can clearly see the splitting of the 220_c reflection (Fig. 6), although in the integrated pattern the line splitting is less pronounced (Fig. 7). Generally in this system (FeO–MgO) the deviation from cubic symmetry is small, and the transition pressure of powder samples is determined by the increase of the FWHM of the 220_c peak compared to the FWHM of the 200_c peak (Mao et al. 2002). Figure 8 shows the pressure variation of the FWHM of the 220_c and 200_c peaks normalized to zero-pressure values. Rapid broadening of the 220_c reflection starts at 35(1) GPa, that we believe to be the transition pressure.

There are several complications in analyzing powder diffraction data under high and non-hydrostatic pressure. The first is a pronounced stress development in the sample chamber of the DAC. On non-hydrostatic compression of a powder sample two principal types of stress develop: uniaxial stress caused by compression between two opposing diamonds, and local stresses that are generated by mismatches in the shapes of neighboring grains in the sample. In angle-dispersive XRD, only crystallites with one particular orientation contribute to the intensity of a particular reflection. This means that each Debye–Scherrer ring is formed by crystallites with different orientations with respect to the stress ellipsoid; hence, each reflection is distorted in different ways. As a result a set of integration parameters to transform 2D XRD images to a single-dimension dataset will be correct for one reflection (i.e., the Debye–Scherrer ring is circular), but not for others (the Debye–Scherrer rings are ellipses). Theories of angle-dispersive XRD under non-hydrostatic conditions predict that uniaxial stress affects diffraction line positions (Dubrovinsky and Dubrovinskaia 2004; Funamori et al. 1997; Singh et al. 1998). Systematic shifts of *d*-spacings for different reflections appear due to inhomogeneous compression of the crystalline solid, which ideally re-

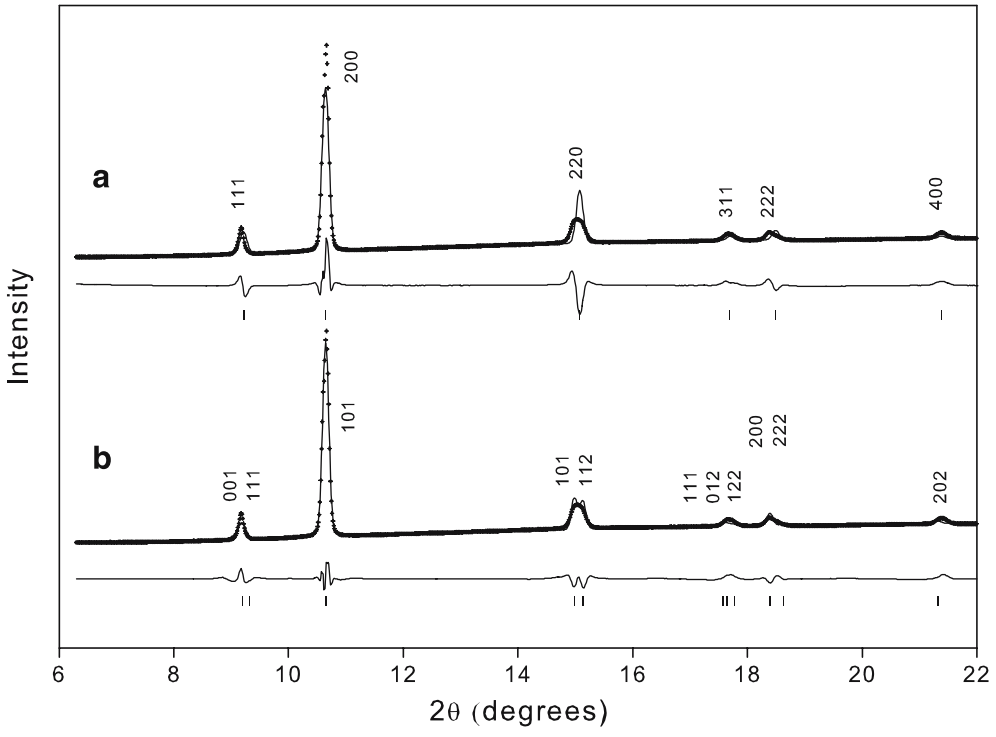

Fig. 7 Full-profile Rietveld refinement of rhombohedral and cubic structures at 41 GPa ($\lambda=0.3738$ Å): **a** Cubic structure (space group $Fm\bar{3}m$) with cell parameter $a=4.029(4)$ Å (*crosses*, experimental data; *solid line*, simulated). Final *R*-factors are $R_p=0.0554$, $R_{wp}=0.0253$, χ^2(reduced) = 4.163. **b** Rhombohedral structure (space group $R\bar{3}m$) with cell parameters $a=2.810(5)$ Å and $\alpha=60.70(1)°$. Final *R*-factors are $R_p=0.0273$, $R_{wp}=0.0145$, χ^2(reduced) = 1.038. In both the cases all fractional atomic coordinates are fixed by symmetry. Mg and Fe atoms were in the same position with occupancies of 0.8 and 0.2, respectively

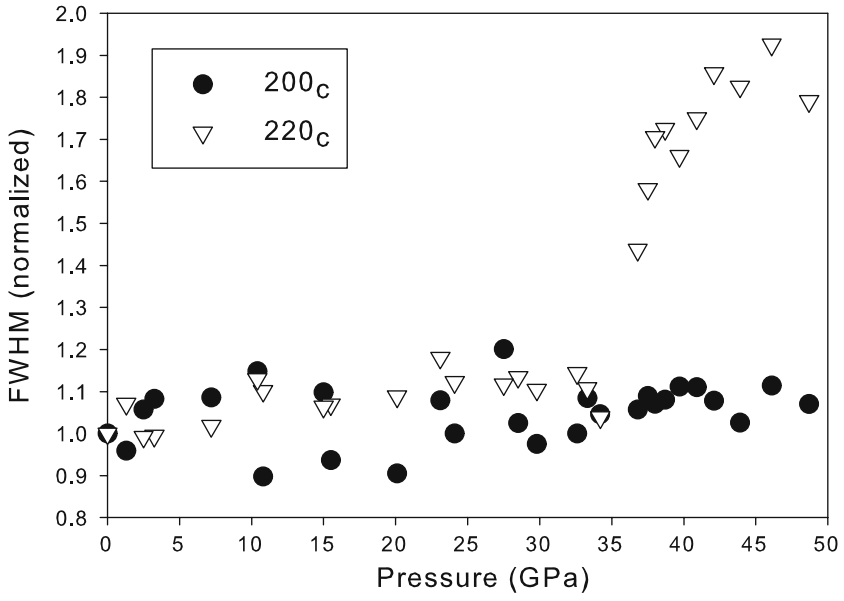

Fig. 8 Full width at half maximum (FWHM) of 200_c and 220_c reflections of $(Mg_{0.8}Fe_{0.2})O$ (normalized to the zero-pressure value) as a function of pressure

quires the complete elastic tensor and uniaxial stress components to account for this effect. Local stress mainly produces broadening of some of the X-ray diffraction lines (Funamori et al. 1997). The second complication is a strong preferred orientation of powder crystallites, which affects the relative peak intensities and also results in intensity variation along each of the Debye–Scherrer rings. For all of these reasons, a full-profile Rietveld refinement is not successful in reproducing the splitting of peaks (see Fig. 7). Instead, we performed an integration of separate peaks over a small area of the image plate with the most pronounced line splitting and without bright spots. The resulting patterns at 42(1) GPa are shown in Fig. 9, which shows clearly that the observed line splitting is consistent with a rhombohedral structure. The rhombohedral angle α, determined from all split reflections, is $60.5 \pm 0.3°$. According to the theories for XRD under non-hydrostatic conditions (Funamori et al. 1997; Singh et al. 1998; Dubrovinsky and Dubrovinskaia 2004), non-hydrostaticity can affect line positions and width, but cannot produce line splitting. Pseudo-splitting can be observed only in the integrated pattern and only when three factors are combined: strong uniaxial stress (e.g., elliptical Debye–Scherrer rings), strong preferred orientation of crystallites in two directions (e.g., bright spots on the nearest and furthest parts of the ellipse) and integration of the entire Debye–Scherrer ring. Line splitting, such as shown in Fig. 6, can only be the result of a reduction in crystal symmetry.

P–V data were fitted to a second-order Birch–Murnagham isothermal equation of state (EOS) with values $K_{300} = 158(5)$ GPa and $V_0 = 11.53(1)$ cm^3/mol for the cubic structure and $K_{300} = 170(7)$ GPa and $V_0 = 11.21(1)$ cm^3/mol for the rhombohedral structure (Fig. 10). According to these parameters, the phase transition from a cubic to a rhombohedral structure appears to be a first order, but with the caveat that no form of EOS can describe *P–V* data accurately near the transition point.

No pressure hysteresis in the phase transition was observed by XRD, and the diffraction pattern of the recovered sample was consistent with the ideal cubic structure.

Discussion

Combined in situ XRD, Mössbauer and XANES spectroscopy data on $(Mg_{0.8}Fe_{0.2})O$ unequivocally indicate a structural transition at 35(1) GPa and room temperature, where the high-pressure phase is interpreted on the basis of Rietveld refinements and line splitting analysis of image-plate data to be a rhombohedral structure. Mössbauer data clearly show the absence of magnetic splitting in spectra from the high-pressure phase to at least 56 GPa, which establishes the stability of the rhombohedral distortion in the absence of magnetic ordering. Similarly, the magnetic ordering transition in FeO was recently shown to occur independently of the rhombohedral structural transition at high pressure and room temperature (Kantor et al. 2004a, b). This decoupling of the rhombohedral distortion from magnetic ordering has important implications for understanding the fundamental interactions in transition metal monoxides. Firstly, the nature of the structural distortion at low temperatures and at high pressures should be reexamined: if the structural transition is not driven by magnetization, another type of interatomic interaction or particular aspects of metal–oxygen chemical bonding may be responsible. Secondly, magnetoelastic coupling in the transition metal monoxides may not be as strong as previously thought (Struzhkin et al. 2001), so that rapid mode softening might not be connected with

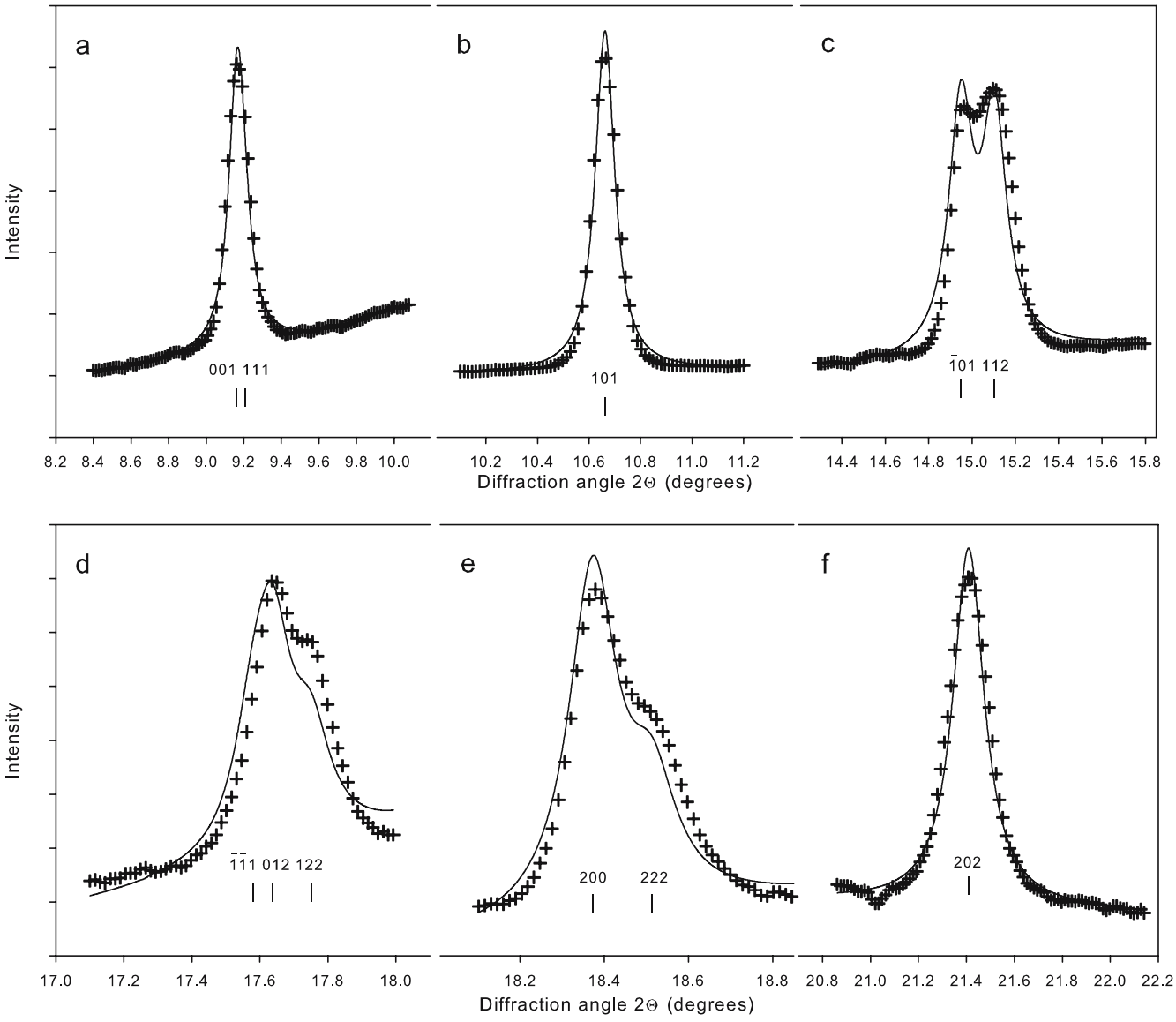

Fig. 9 X-ray diffraction patterns collected at 42(1) GPa showing splitting of former cubic reflections: **a** 111_c, **b** 200_c, **c** 220_c, **d** 311_c, **e** 222_c, and **f** 400_c. *Crosses*, experimental intensity; *solid lines*, calculated for a rhombohedral structure with $\alpha \approx 60.4°$. *Ticks and indices* below curves show the positions of rhombohedral reflections

magnetic interactions, but only with the structural phase transition.

The composition $x_{Fe} = 0.2$ is the lowest iron concentration in (Mg,Fe)O so far where a cubic-to-rhombohedral phase transition has been reported (Fig. 11). However comparison of results from different laboratories is complicated by two factors: (1) experimental resolution must exceed a certain value in order to detect the transition and (2) the effect of non-hydrostatic stress on the phase transition. Hence, the observation that no phase transition occurs in the compositions $x_{Fe} = 0.4$ (Shu et al. 1998b) and $x_{Fe} = 0.6$ (Lin et al. 2003; Richet et al. 1989) could also be interpreted to indicate that experimental resolution was not sufficient to observe the transition. For example in the present study the presence of the transition could not be confirmed using only the integrated X-ray diffraction patterns (see above). Also, the presence of overlapping peaks from the pressure medium, e.g., NaCl (Lin et al. 2003) can also reduce experimental resolution.

Non-hydrostatic stress likely affects the pressure of the structural transition in (Mg,Fe)O. Previous experiments have already demonstrated that the degree of non-hydrostaticity affects the structural transition pressure in FeO (Dubrovinsky et al. 2000a), and comparison of previous experimental results for (Mg,Fe)O shows a trend to increasing transition pressure as the degree of non-hydrostatic stress in the experiment is reduced (Fig. 11). Non-hydrostatic stress can also change the nature of the transition, e.g., a second-order transition becomes a tricritical under stress in MnO (Bloch et al. 1975).

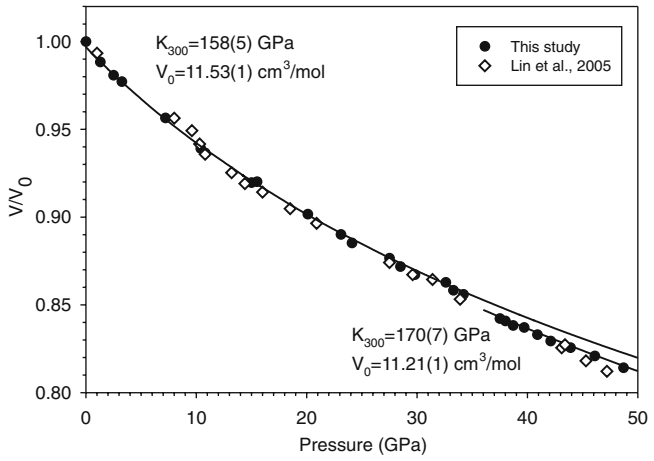

Fig. 10 Pressure–volume data for sample FP-1 (*black circles*). Fits to a second-order Birch–Murnaghan equation of state are shown as *solid lines*. Data for $(Mg_{0.83}Fe_{0.17})O$ from Lin et al. (2005) are placed for comparison (*open diamonds*)

The observed high-pressure X-ray diffraction patterns indicate a lowering of crystal symmetry, and cannot be described as a cubic phase under non-hydrostatic stress as discussed in Results. On the other hand, the cubic-to-rhombohedral transition could be driven by uniaxial stress; in other words, the transformation could be stress induced. Since the degree of pseudo-cubic lattice distortion is known, a strain tensor can be easily calculated. However in order to transform the strain tensor into a stress tensor, the full single-crystal elastic tensor is required, which is unknown for $(Mg_{0.8}Fe_{0.2})O$ ferropericlase under high pressure. In order to make estimations of stress tensor components, we used elastic constants of pure MgO, which are well determined at high pressure (Zha et al. 2000). This calculation shows that a uniaxial stress of about 3 GPa is required to produce a corresponding ($\alpha = 60.5°$) rhombohedral distortion of the cubic lattice at 40 GPa. The magnitude of this stress is within values expected for DAC experiments conducted without a pressure medium (Merkel et al. 2002); hence, stress development could be a driving mechanism for the phase transition. However, the electronic structure is also a factor, because no evidence of a rhombohedral distortion has been observed in pure MgO (Duffy et al. 1995; Merkel et al. 2002) even at extreme pressures and under high uniaxial stress.

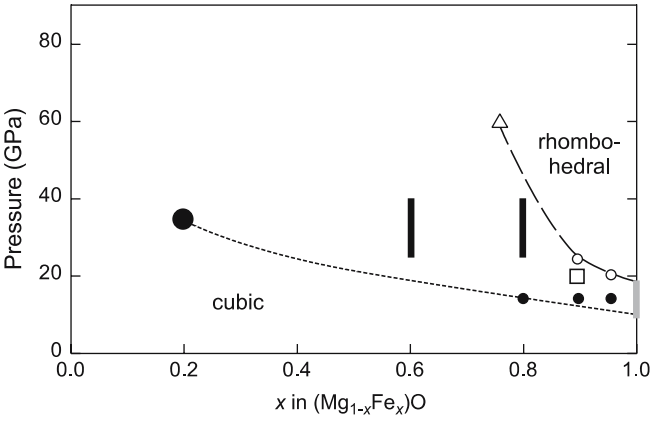

Fig. 11 Phase diagram for (Mg,Fe)O at room temperature showing the cubic–rhombohedral phase boundary. *Solid symbols* represent experiments where non-hydrostatic stress is large, while *open symbols* indicate experiments where a pressure medium was used and non-hydrostatic stress is inferred to be less. *Small solid circles* (Kondo et al. 2004), *black bars and open circles* (Shu et al. 1998b), *triangle* (Lin et al. 2003), *square* (Mao et al. 2002) *large solid circle*, this work; *grey bar*, range of transition pressures observed in FeO using different types of pressure media (Shu et al. 1998a; Yagi et al. 1985). The *dotted line* indicates the inferred phase boundary for experiments conducted under conditions of large non-hydrostatic stress, while the *dashed line* indicates the boundary inferred for experiments where non-hydrostatic stress is significantly less. Results from experiments where no cubic–rhombohedral transition was observed are not shown on the plot due to the ambiguity of whether experimental resolution was sufficient to distinguish the rhomboderal distortion (see the text)

Conclusions

On the basis of this study, we have clearly shown that 20 mol% FeO is sufficient to induce a rhombohedral distortion in (Mg,Fe)O at a confining pressure of ~35 GPa in the presence of uniaxial stress. It is also clear from MS that the rhombohedral distortion of $Mg_{0.8}Fe_{0.2}O$ is not associated with long-range magnetic ordering. A rhombohedral distortion in ferropericlase with mantle composition ($Mg_{0.8}Fe_{0.2}O$) could influence physical properties of the Earth's lower mantle, since such a phase transition is accompanied by a rapid C_{44} mode softening (Sumino et al. 1980) and by a decrease of sound wave velocities.

Acknowledgement This study was partly supported by DFG, RFBR, Russian Federation Government support of the leading scientific schools, Swedish Research council (VR), and CNPq (Brazil). The authors would also like to acknowledge G. Hermannsdorfer and H. Fischer for their technical support.

References

Ankudinov AL, Bouldin CE, Rehr JJ, Sims J, Hung H (2002) Parallel calculation of electron multiple scattering using Lanczos algorithms. Phys Rev B 65:104–107

Ankudinov AL, Ravel B, Rehr JJ, Conradson SD (1998) Real-space multiple-scattering calculation and interpretation of x-ray-absorption near-edge structure. Phys Rev B 58:7565–7576

Badro J, Fiquet G, Guyot F, Rueff JP, Struzhkin VV, Vankó G, Monaco G (2003) Iron partitioning in Earth's mantle: toward a deep lower mantle discontinuity. Science 300:789–791

von Barth U, Grossmann G (1982) Dynamical effects in x-ray spectra and the final-state rule. Phys Rev B 25:5150–5179

Bloch D, Hermann-Ronzaud D, Vettier C, Yelon WB, Alben R (1975) Stress-induced tricritical phase transition in manganese oxide. Phys Rev Lett 35:963–967

Dobson DP, Cohen NS, Pankhurst QA, Brodholt JP (1998) A convenient method for measuring ferric iron in magnesiowustite ($MgO–Fe_{1-x}O$). Am Miner 83:794–798

Dubrovinskaia N, Dubrovinsky L (2003) Whole-cell heater for the diamond anvil cell. Rev Sci Instr 74:3433–3437

Dubrovinsky L, Dubrovinskaya N (2004) Angle-dispersive diffraction under non-hydrostatic stress in diamond anvil cells. J All Comp 375:86–92

Dubrovinsky L, Dubrovinskaia N, Saxena S, LiBehan T (2000a) X-ray diffraction under non-hydrostatic conditions in experiments with diamond anvil cell: wustite (FeO) as an example. Mater Sci Eng A 288:187–190

Dubrovinsky LS, Dubrovinskaia NA, Saxena SK, Annersten H, Hålenius E, Harryson H, Tutti F, Rekhi S, Le Bihan T (2000b) Stability of ferropericlase in the lower mantle. Science 289:430–432

Duffy TS, Hemley RJ, Mao HK (1995) Equation of state and shear strength at multimegabar pressures: magnesium oxide to 227 GPa. Phys Rev Lett 74:1371–1374

Fang Z, Solovyev IV, Sawada H, Terakura K (1999) First-principle study on electronic structures and phase stability of MnO and FeO under high pressure. Phys Rev B 59:762–774

Funamori N, Funamori M, Jeanloz R, Hamaya N (1997) Broadening of x-ray powder diffraction lines under nonhydrostatic stress. J Appl Phys 82:142–146

Gale JD (1997) GULP—a computer program for the symmetry adapted simulation of solids. J Chem Soc, Faraday Trans 4:629–637

Gramsch SA, Cohen RE, Savrasov SY (2003) Structure, metal–insulator transitions, and magnetic properties of FeO at high pressures. Am Miner 88:257–261

Guo QZ, Mao HK, Hu J, Shu J, Hemley RJ (2002) The phase transitions of CoO under static pressure to 104 GPa. J Phys: Condens Matter 14:11369–11374

Hedin L, Lundqvist BI (1971) Explicit local exchange-correlation potentials. J Phys C 4:2064–2083

Kantor AP, Jacobsen SD, Kantor IYu, Dubrovinsky LS, McCammon CA, Reichmann HJ, Goncharenko IN (2004a) Pressure-induced magnetization in FeO: evidence from elasticity and Mössbauer spectroscopy. Phys Rev Lett 93:215502

Kantor IYu, McCammon CA, Dubrovinsky LS (2004b) Mossbauer spectroscopic study of pressure-induced magnetisation in wiistite (FeO). J All Comp 376:5–8

Kantor IYu, Dubrovinsky LS, Kantor AP, Urusov VS, McCammon C, Crichton W (2005) Trigonal distortion of ferropericlase ($Mg_{0.8}Fe_{0.2}$)O at high pressures. Dokl Phys 50:343–345

Kizler P (1992) X-ray-absorption near-edge structure spectra for bulk materials: multiple-scattering analysis versus a phenomenological approach. Phys Rev B 46:10540–10546

Kondo T, Ohtani E, Hirao N, Yagi T, Kikegawa T (2004) Phase transitions of (Mg,Fe)O at megabar pressures. Phys Earth Planet Int 201:143–144

Kondo T, Ohtani E, Yagi T, Kikegawa T (2002) In-situ X-ray study of (Mg,Fe)O under high pressure and temperature. J Conf Abstr 7:57

Kuzmin A, Mironova N, Purans J (1997) The influence of pd mixing and magnetic interactions on the pre-edge peak intensity at the Co (Ni) K absorption edge in Co(Ni)cMg1–cO solid solutions. J Phys: Condens Matter 9:5277–5286

Lin JF, Heinz DL, Mao HK, Hemley RJ, Devine JM, Li J, Shen G (2003) Stability of magnesiowustite in Earth's lower mantle. Proc Natl Acad Sci USA 100:4405–4408

Lin JF, Struzhkin VV, Jacobsen SD, Hu MY, Chow P, Kung J, Liu H, Mao HK, Hemley RJ (2005) Spin transition of iron in magnesiowüstite in the Earth's lower mantle. Nature 436:377–380

Lytle FW, Greegor RB, Panson AJ (1988) Discussion of x-ray-absorption near-edge structure: application to Cu in the high-T_c superconductors $La_{1.8}Sr_{0.2}CuO_4$ and $YBa_2Cu_3O_7$. Phys Rev B 37:1550–1562

Mao W, Shu J, Hu J, Hemley R, Mao HK (2002) Displacive transition in magnesiowustite. J Phys: Condens Matter 14:11349–11354

Mao HK, Xu J, Bell PM (1986) Calibration of the ruby pressure gauge to 800 kbar under quasihydrostatic conditions. J Geophys Res 91:4673–4678

McCammon CA, Tennant C (1996) High-pressure Mössbauer study of synthetic clinoferrite, FeSiO3. "Mineral spectroscopy: a tribute to Roger G. Burns", Special publication no. 5, Geochemical Society, Houston, pp 281–288

McCammon C, Peyronneau J, Poirier J-P (1998) Low ferric iron content of (Mg,Fe)O at high pressures and temperatures. Geophys Res Lett 25:1589–1592

Merkel S, Wenk HR, Shu J, Shen G, Gillet P, Mao HK, Hemley RJ (2002) Deformation of polycrystalline MgO at pressures of the lower mantle. J Geophys Res 107:2271–2288

Minervini L, Grimes RW (1999) Defect clustering in wüstite. J Phys Chem Solids 60:235–245

Morosin B (1970) Exchange Striction Effects in MnO and MnS. Phys Rev B 1:236–243

Nasu S (1994) High pressure Mössbauer spectroscopy using a diamond anvil cell. Hyperfine Inter 90:59–75

Pascarelli S, Mathon O, Aquilanti G (2004) New opportunities for high pressure X-ray absorption spectroscopy using dispersive optics. J All Comp 362:33–40

Rehr JJ, Albers RC (2000) Theoretical approaches to x-ray absorption fine structure. Rev Mod Phys 72:621–654

Richet P, Mao HK, Bell PM (1989) Bulk moduli of magnesiowustites from static compression measurements. J Geophys Res 94:3037–3045

Rooksby HP (1948) A note on the structure of nickel oxide at subnormal and elevated temperatures. Acta Cryst 1:226

Saito S, Nakahigashi K, Shimomura Y (1966) X-ray diffraction study on CoO. J Phys Soc Jpn 21:850–860

Shu J, Mao HK, Hu J, Fei Y, Hemley RJ (1998a) Single-crystal X-ray diffraction of wustite to 30 GPa hydrostatic pressure. N Jb Miner Abh 172:309–323

Shu J, Mao HK, Hu J, Fei Y, Hemley RJ (1998b) High-pressure phase transition in magnesiowustite ($Fe_{1-x}Mg_x$)O. EOS Trans Am Geophys Union 79(17); Spring Meeting Suppl:M21A-01

Singh AK, Mao HK, Shu J, Hemley RJ (1998) Estimation of single-crystal elastic moduli from polycrystalline X-ray diffraction at high pressure: application to FeO and iron. Phys Rev Lett 80:2157–2160

Smart JS, Greenwald S (1951) Crystal structure transitions in antiferromagnetic compounds at the Curie temperature. Phys Rev 82:113–114

Srivastava UC, Nigam HL (1973) X-ray absorption edge spectrometry (XAES) as applied to coordination chemistry. Coord Chem Rev 9:275–310

Struzhkin VV, Mao HK, Hu J, Schwoerer-Böhning M, Shu J, Hemley RJ, Sturhahn W, Hu MY, Alp EE, Eng P, Shen G (2001) Nuclear inelastic X-ray scattering of FeO to 48 GPa. Phys Rev Lett 87:255501

Sumino Y, Kumazawa M, Nishizawa O, Pluschkell W (1980) The elastic constants of single-crystal $Fe_{1-x}O$, MnO and CoO, and the elasticity of stochiometric magnesiowuitite. J Phys Earth 28:475–495

Wentzcovitch RM, Karki BB, Cococcioni M, deGironcoli S (2004) Thermoelastic properties of $MgSiO_3$-Perovskite: insights on the nature of the Earth's lower mantle. Phys Rev Lett 92:018501

Willis BTM, Rooksby HP (1953) Change of structure of ferrous oxide at low temperature. Acta Cryst 6:827–831

Yagi T, Suzuki T, Akimoto SI (1985) Compression of wustite ($Fe_{0.98}O$) to 120 GPa. J Geophys Res 90:8784–8788

Yoo CS, Maddox B, Klepeis J-HP, Iota V, Evans W, McMahan A, Hu MY, Chow P, Somayazulu M, Häusermann D, Scalettar RT, Pickett WE (2005) First-order isostructural Mott transition in highly compressed MnO. Phys Rev Lett 94:115502

Zabinsky SI, Rehr JJ, Ankudinov A, Albers RC, Eller MJ (1995) Multiple-scattering calculations of x-ray-absorption spectra. Phys Rev B 52:2995–3009

Zha CS, Mao HK, Hemley RJ (2000) Elasticity of MgO and a primary pressure scale to 55 GPa. Proc Natl Acad Sci USA 97:13494–13499